A Unified Description of the Electrochemical, Charge Distribution, and Spectroscopic Properties of the Special-Pair Radical Cation in Bacterial Photosynthesis

Jeffrey R. Reimers*,[†] and Noel S. Hush[†,‡]

Contribution from the School of Chemistry and the School of Molecular and Microbial Biosciences, The University of Sydney, NSW 2006, Australia

Received June 24, 2003; E-mail: reimers@chem.usyd.edu.au

Abstract: We apply our four-state 70-vibration vibronic-coupling model for the properties of the photosynthetic special-pair radical cation to: (1) interpret the observed correlations between the midpoint potential and the distribution of spin density between the two bacteriochlorophylls for 30 mutants of *Rhodobacter sphaeroides*, (2) interpret the observed average intervalence hole-transfer absorption energies as a function of spin density for six mutants, and (3) simulate the recently obtained intervalence electroabsorption Stark spectrum of the wild-type reaction center. While three new parameters describing the location of the sites of mutation with respect to the special pair are required to describe the midpoint-potential data, a priori predictions are made for the transition energies and the Stark spectrum. In general, excellent predictions are made of the observed quantities, with deviations being typically of the order of twice the experimental uncertainties. A unified description of many chemical and spectroscopic properties of the bacterial reaction center is thus provided. Central to the analysis is the assumption that the perturbations made to the reaction center, either via mutations of protein residues or by application of an external electric field, act only to independently modify the oxidation potentials of the two halves of the special pair and hence the redox asymmetry E_0. While this appears to be a good approximation, clear evidence is presented that effects of mutation can be more extensive than what is allowed for. A thorough set of analytical equations describing the observed properties is obtained using the Born–Oppenheimer adiabatic approximation. These equations are generally appropriate for intervalence charge-transfer problems and include, for the first time, full treatment of both symmetric and antisymmetric vibrational motions. The limits of validity of the adiabatic approach to the full nonadiabatic problem are obtained.

1. Introduction

In bacterial, algal, and plant photosynthesis, a key element involved in the primary charge-separation process that converts optical to electrical energy en route to chemical energy is a weakly to strongly coupled dimer known as the special-pair P.[1] This species forms either all or part of the primary electron donor in these systems and is comprised of either chlorophyll or bacteriochlorophyll molecules. While detailed information is becoming available for the plant photosystems PS-I and PS-II, much more is known about the function of the special pair in bacterial photosystems. Therein, it is a strongly coupled dimer whose properties control the charge-separation process, and much can be learned about the plant photosystems through understanding of the inherent differences.[2] Our purpose here is to provide a unified description of the detailed electrochemical midpoint potentials, ENDOR spin distributions,[3–7] and spectro-

scopic[7–10] properties of the bacterial special pair including the revealing recent electroabsorption Stark spectrum[11] of the special-pair radical cation P^+, the species produced upon charge separation. From this, a basic understanding of the operation of the special pair is obtained, including an understanding of the effects of perturbations of its external environment through both the application of external electric fields and site-directed mutagenesis.

The special-pair radical cation has many properties analogous to those of the mixed-valence complexes such as the Creutz–Taube ion[12] whose study has been very important in the development of electron-transfer theory. Of utmost importance in such systems is the internal charge distribution;[13–15] for the

---

† School of Chemistry.
‡ School of Molecular and Microbial Biosciences.
(1) Hoff, A. J.; Deisenhofer, J. *Phys. Rep.* **1997**, *287*, 1.
(2) Reimers, J. R.; Shapley, W. A.; Hush, N. S. *J. Chem. Phys.* **2003**, *119*, 3240.
(3) Lin, X.; Murchisson, H. A.; Nagarajan, V.; Parson, W. W.; Allen, J. P.; Williams, J. C. *Proc. Natl. Acad. Sci. U.S.A.* **1994**, *91*, 10265.
(4) Artz, K.; Williams, J. C.; Allen, J. P.; Lendzian, F.; Rautter, J.; Lubitz, W. *Proc. Natl. Acad. Sci. U.S.A.* **1997**, *94*, 13582.

(5) Ivancich, A.; Artz, K.; Williams, J. C.; Allen, J. P.; Mattioli, T. A. *Biochemistry* **1998**, *37*, 11812.
(6) Müh, F.; Lendzian, F.; Roy, M.; Williams, J. C.; Allen, J. P.; Lubitz, W. *J. Phys. Chem. B* **2002**, *106*, 3226.
(7) Johnson, E. T.; Müh, F.; Nabedryk, E.; Williams, J. C.; Allen, J. P.; Lubitz, W.; Breton, J.; Parson, W. W. *J. Phys. Chem. B* **2002**, *106*, 11859.
(8) Breton, J.; Nabedryk, E.; Parson, W. W. *Biochemistry* **1992**, *31*, 7503.
(9) Nabedryk, E.; Allen, J. P.; Taguchi, A. K. W.; Williams, J. C.; Woodbury, N. W.; Breton, J. *Biochemistry* **1993**, *32*, 13879.
(10) Breton, J.; Nabedryk, E.; Clérici, A. *Vib. Spectrosc.* **1999**, *19*, 71.
(11) Treynor, T. P.; Andrews, S. S.; Boxer, S. G. *J. Phys. Chem.* **2003**, *107*, 11230.
(12) Creutz, C.; Taube, H. *J. Am. Chem. Soc.* **1969**, *91*, 3988.
(13) Allen, G. C.; Hush, N. S. *Prog. Inorg. Chem.* **1967**, *8*, 357.
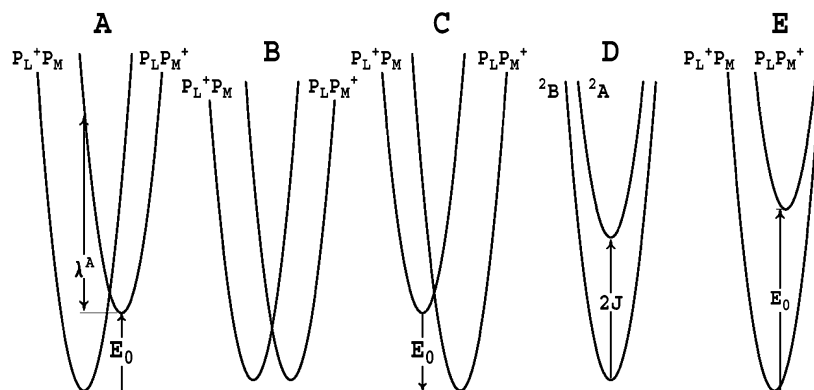(14) Hush, N. S. *Prog. Inorg. Chem.* **1967**, *8*, 391.

Figure 1. Sketch of the diabatic potential-energy surfaces for intervalence charge-transfer processes that are most characteristic of the adiabatic ones in various regimes: A for $|2J| < \lambda^A$, $E_0 > 0$; B for $|2J| < \lambda^A$, $E_0 = 0$; C for $|2J| < \lambda^A$, $E_0 < 0$; D for $2J > \lambda^A$ and $|2J| > E_0$; and E for $\lambda^A < |2J| < E_0$.

case of bacterial photosynthesis, this amounts to whether the positive charge is localized on one of the two monomers or delocalized over both. If the charge is localized, then one can construct two potential-energy surfaces for the dimer, one for $P_L^+P_M$ and another for $P_LP_M^+$, where P_L and P_M are the individual bacteriochlorophyll molecules that comprise the dimer P.[1] Sample potential-energy surfaces are shown in Figure 1 for the three possible charge-localized scenarios: case A, asymmetric dimer with the charge on P_L; case B, symmetric dimer in which external fluctuations and past history control the instantaneous localization (over a long-time average the charge is equally distributed); and case C, asymmetric dimer with the charge on P_M. Control over these scenarios[16,17] is affected by the redox asymmetry E_0 (often also identified as the driving force "ΔG_0") shown in the figure, which is positive for case A, zero for case B (this applies, e.g., for the Creutz–Taube ion and most symmetric inorganic or organic molecular systems), and negative for case C. In photosynthetic reaction-center proteins, E_0 is controlled by asymmetric electric fields originating from the surrounding protein, as well as from internal conformational differences of the bacteriochlorophyll halves.[5–7,18–23] The chemical drive for the charge to localize in one of these ways is also provided by the antisymmetric-mode reorganization energy λ^A.[24] This is the energy that is released when a fully charge-localized system in the electronic configuration for one species (say $P_L^+P_M$) relaxes from the equilibrium geometry of the other species (thence $P_LP_M^+$) to its native equilibrium geometry, see Figure 1. Opposing such localization is the electronic interaction J between the two halves of the dimer. Such an interaction is directly analogous to the well-known interaction between two hydrogen atoms as they are brought together,[25] an interaction which in that case leads to the delocalization of the electrons and the formation of the

covalent bond. In reaction centers, if $2|J|$ exceeds both λ^A and E_0, then the drive to delocalize the positive charge over both halves exceeds that to localize it;[24] the most apt potential-energy surfaces for the problem become the delocalized surfaces ^{2}B (predicted by calculations[26] to be the ground state for bacterial photosynthetic special pairs) and ^{2}A as indicated as case D in Figure 1. Note that the symmetry designators used here reflect the pseudo-C_2 symmetry of the photosynthetic reaction center.[1] The situation in which localization is induced by the asymmetry E_0 is depicted in case E for which $E_0 > 2|J| > \lambda^A$.

Understanding the chemical properties of the special-pair radical cation, and how external modulations of the system operate, thus requires determination of the values of J, λ^A, and E_0 for the reaction centers. For *Rhodobacter* (*Rb.*) *sphaeroides*, the most reliable values currently available are $J = 0.126 \pm 0.002$ eV, $\lambda^A = 0.139 \pm 0.003$ eV, and $E_0 = 0.069 \pm 0.002$ eV, obtained from our four-state 70-vibration analysis of the low-resolution and medium-resolution aspects of the observed intervalence hole-transfer spectrum.[10] This spectrum was first observed by Breton, Nabedryk, and Parson[8] and provides detailed information concerning the properties of P^+. These properties can change dramatically as J, λ^A, and E_0 vary, as is implied from an examination of the manifold of spectra obtained so far for plant photosystems.[2]

The complexity (and hence usefulness) of the intervalence-hole-transfer spectrum arises as the motion of the positive charge (the electron hole) is strongly coupled to nuclear motion: as the nuclei vibrate along the generalized coordinate shown in Figure 1, the electron hole is dragged with them.[13,14] During hole-transfer absorption, optical energy is used to convert, in the localized description, $P_L^+P_M$ to $P_LP_M^+$, or, in the delocalized description, ^{2}B to ^{2}A; this electronic transition is observed over the range of 2000–5000 nm (or 2000–5000 cm^{-1}) in the infrared region of the spectrum rather than in the 200–800 nm region typical of electronic transitions in molecules. Further, the coupling between the location of the positive charge and the nuclear motions gives rise to extremely intense vibrational infrared absorptions for the individual vibrational modes that comprise this generalized coordinate. Such absorptions are known as phase-phonon lines following the pioneering studies of Rice et al.[27–30] As the means of intensification of these

(15) Hush, N. S. *NATO Adv. Study Inst. Ser., Ser. C* **1980**, *58*, 151.
(16) Marcus, R. A. *J. Chem. Phys.* **1957**, *26*, 867.
(17) Hush, N. S. *J. Chem. Phys.* **1958**, *28*, 962.
(18) Alden, R. G.; Parson, W. W.; Chu, Z. T.; Warshel, A. *J. Am. Chem. Soc.* **1995**, *117*, 12284.
(19) Muegge, I.; Apostolakis, J.; Ermler, U.; Fritzsch, G.; Lubitz, W.; Knapp, E. W. *Biochemistry* **1996**, *35*, 8359.
(20) Gunner, M. R.; Nicholls, A.; Honig, B. *J. Phys. Chem.* **1996**, *100*, 4277.
(21) Sakuma, T.; Kashiwagi, H.; Takada, T.; Nakamura, H. *Int. J. Quantum Chem.* **1997**, *61*, 137.
(22) Hughes, J. M.; Hutter, M. C.; Reimers, J. R.; Hush, N. S. *J. Am. Chem. Soc.* **2001**, *123*, 8550.
(23) Reimers, J. R.; Hughes, J. M.; Hush, N. S. *Biochemistry* **2000**, *39*, 16185.
(24) Hush, N. S. *Chem. Phys.* **1975**, *10*, 361.
(25) Bacskay, G. B.; Reimers, J. R.; Nordholm, S. *J. Chem. Educ.* **1997**, *74*, 1494.

(26) Reimers, J. R.; Shapley, W. A.; Rendell, A. P.; Hush, N. S. *J. Chem. Phys.* **2003**, *119*, 3249.
(27) Rice, M. J. *Phys. Rev. Lett.* **1976**, *37*, 36.
(28) Rice, M. J.; Lipari, N. O.; Strässler, S. *Phys. Rev. Lett.* **1977**, *39*, 1359.

transitions is different from that which normally facilitates vibrational infrared spectroscopy, very unusual phenomena occur. In particular, the most intense phase-phonon lines observed for the special-pair radical cation have been assigned[26] to coupled motions of pseudo *g* symmetry on each individual bacteriochlorophyll, motions that are naively expected to give rise to weak infrared absorptions and indeed are not observed in the infrared spectra of either the bacteriochlorophyll neutral or cationic monomers or the neutral special pair.

Initially,[8,9] only three phase-phonon lines were readily distinguished in the observed spectra, and they quickly proved to be a major focus of attention. As the observed spectra are typically not simply the spectrum of P⁺ but rather the difference spectrum between this radical cation and the neutral species P,[8] phase-phonon activity is difficult to separate from the effects of simple vibrational frequency changes due to oxidation. To complicate this even further, vibrations whose frequency changes on oxidation may also be associated with phase-phonon activity. We have developed a technique[31] of artificially broadening observed spectra to eliminate the effects of frequency modulation and hence expose the qualitative nature of the phase-phonon lines. This technique, combined with the recent extension of the observable spectral range down to 300 cm⁻¹,[10] indicate that actually a very large number of vibrational modes are associated with phase-phonon activity, modes that somewhat uniformly span the $300-1600$ cm⁻¹ region.

Coupling between electronic and nuclear motions is known as vibronic[32] or electron-phonon coupling. It gives rise to breakdown of the Born−Oppenheimer approximation[33] that allows molecules to be considered simply as nuclei moving in potential-energy fields supplied by the electrons − the approximation that sits at the heart of the modern conceptual framework for chemical reactivity and spectroscopy. While in most instances breakdown of the Born−Oppenheimer approximation leads to only minor spectroscopic perturbations, for intervalence charge-transfer problems, the effects may be profound enough to dominate observed properties. Indeed, as for photosynthetic systems, the intervalence electronic absorption spectrum appears within the range of the normal vibrational infrared transitions, and the vibronic effects are expected to dominate. Also, non-Born−Oppenheimer (or nonadiabatic) effects in intervalence spectroscopy are most important when $2|J| \approx \lambda^A$, the approximate operating point for bacterial and PS-I photosynthesis.

One particular application for which nonadiabatic effects are critical is in the determination of the electroabsorption Stark spectrum.[11] This is a century-old experimental technique, the recent refinement of which by Boxer has brought about a renaissance that has had profound effects on fields from inorganic chemistry[34] to photosynthesis.[34−37] A large external electric field (often in excess of 3 MV cm⁻¹) is applied to the

system, and the change in the absorption spectrum is measured directly. Using Born−Oppenheimer theory, this spectrum is usually interpreted in terms of the equations of Liptay[38−42] and typically gives an immediate and unambiguous diagnosis of the nature of the degree of electron localization. However, this approach becomes ineffective when significant Born−Oppenheimer breakdown occurs, as complex and misleading spectra are then obtained.[43] Proper analysis of the recent spectrum of the special-pair radical cation obtained by Treynor, Andrews, and Boxer[11] requires a nonadiabatic approach.

Indeed, simulation of the intervalence spectrum itself[14] requires a nonadiabatic treatment such as the PKS model[44] or related approaches.[11,45−47] For bacterial photosynthesis, prior calculations have by necessity relied on simplistic models derived from ad hoc assumptions concerning the nature of the coupled modes, but recently we have presented a realistic, extensive description of the vibronic coupling.[31] While model calculations are useful and revealing, particularly when the correct region of the $J-\lambda^A-E_0$ parameter space in which they need to operate is already known,[11] they cannot be used to determine that region themselves.[46] In this work, only the extensive vibrational description is applied.

For the special-pair radical cation of bacterial photosynthesis, a complication is the presence of an additional electronic transition involving second-highest-occupied molecular orbital (SHOMO) to highest-occupied molecular orbital (HOMO) nature observed as a shoulder at 2200 cm⁻¹ on the red side of the hole-transfer band maximum. This transition is intrinsically too weak to be observed in the spectra of monomeric bacteriochlorophylls (they are forbidden in porphyrin), but for the special-pair radical cation it becomes intensified through strong vibronic coupling with the hole-transfer state.[26] Associated with it is another state of similar nature that is not so intensified and hence is not readily identifiable in the absorption spectrum. Our model[31] for the properties of the special-pair radical cation includes these two states as well as the ground state and hole-transfer state, making it a four-state model. It is the first model to fully include all of the key spectroscopic features.

Central to quantitative modeling of the hole-transfer absorption spectrum is specification of the nature of the generalized antisymmetric nuclear coordinate depicted in Figure 1. In our model,[31] this was established using density-functional theory to determine the number of coupled vibrational modes, their frequencies, and vibronic-coupling constants. In its final form, 50 antisymmetric modes were included, and in addition 20 symmetric modes were also included, making 70 vibrational modes total. These results reflect the key experimental observations[10] that the vibronic coupling is widely distributed among a large number of different antisymmetric modes spanning a wide frequency range, with there being also detectable symmetric-

(29) Rice, M. J. *Solid State Commun.* **1979**, *31*, 93.
(30) Rice, M. J.; Yartsev, V. M.; Jacobsen, C. S. *Phys. Rev. B* **1980**, *21*, 3437.
(31) Reimers, J. R.; Hush, N. S. *J. Chem. Phys.* **2003**, 3262.
(32) Fischer, G. *Vibronic Coupling: The Interaction between the Electronic and Nuclear Motions*; Academic Press: London, 1984.
(33) Born, M.; Oppenheimer, R. *Ann. Phys.* **1927**, *84*, 457.
(34) Oh, D. H.; Sano, M.; Boxer, S. G. *J. Am. Chem. Soc.* **1991**, *113*, 6880.
(35) Lockhart, D. J.; Kirmaier, C.; Holten, D.; Boxer, S. G. *J. Phys. Chem.* **1990**, *94*, 6987.
(36) Steffen, M. A.; Lao, K.; Boxer, S. G. *Science* **1994**, *264*, 810.
(37) Zhou, H.; Boxer, S. G. *J. Phys. Chem. B* **1998**, *102*, 9139.

(38) Liptay, W. *Z. Naturforsch., A: Phys. Sci.* **1965**, *20*, 272.
(39) Liptay, W. *Angew. Chem., Int. Ed. Engl.* **1969**, *8*, 177.
(40) Liptay, W. In *Excited States*; Lim, E. C., Ed.; Academic Press: New York, 1974; p 129.
(41) Varma, C. A. G. O. *Helv. Chim. Acta* **1978**, *61*, 773.
(42) Lin, S. H. *J. Chem. Phys.* **1975**, *62*, 4500.
(43) Reimers, J. R.; Hush, N. S. In *Mixed Valence Systems: Applications in Chemistry, Physics, and Biology*; Prassides, K., Ed.; Kluwer Acad. Publishers: Dordrecht, 1991; p 29.
(44) Piepho, S. B.; Krausz, E. R.; Schatz, P. N. *J. Am. Chem. Soc.* **1978**, *100*, 2996.
(45) Reimers, J. R.; Hush, N. S. *Chem. Phys.* **1995**, *197*, 323.
(46) Reimers, J. R.; Hush, N. S. *Chem. Phys.* **1996**, *208*, 177; erratum *Chem. Phys.* **2004**, *299*, 79.
(47) Gasyna, Z.; Schatz, P. N. *J. Phys. Chem.* **1996**, *100*, 1445.

mode activity but no identifiable progressions in any one particularly significant mode. The reliance on computed properties clearly limits the ability of our model to quantitatively describe individual mode-specific effects,[31] but forms an essential part of the usage of the model in determining the primary qualitative features of the special-pair radical cation.

Computationally, evaluation of the absorption spectrum when a large number of modes are coupled is not trivial as the order of difficulty of solution increases exponentially with the number of modes, and previously only at most two modes had been simultaneously considered in photosynthetic reaction-center applications. To implement an extensive quantitative approach to spectral simulation, we thus developed new techniques for the spectral evaluation appropriate for use with 70 modes.[31] These techniques not only result in the dramatic reduction of the number of quanta of excitation required in each vibrational mode and hence the dimension of the vibronic Hamiltonian matrix, but also facilitate evaluation of the absorption spectrum in such a way that the required computer time scales nearly linearly rather than cubically with the matrix dimension. Initially,[31] this method was applied to deduce the controlling parameters J, λ^A, and E_0 and others describing the SHOMO → HOMO transitions by fitting the observed intervalence spectrum. Here, we apply this four-state 70-mode model to determine the redox midpoint potential, the degree of charge localization, and the intervalence spectral transition energy for a variety of mutant reaction centers of *Rb. sphaeroides*, simulating also the observed Stark electroabsorption spectrum of Treynor, Andrews, and Boxer.[11] The dimension of the Hamiltonian matrix used is 2×10^6, and the spectral simulations performed require 10 min CPU time each on a Pentium-IV/1800 computer.[31]

Historically, the concept that observed midpoint potentials and spin localizations for homologous series of mutant reaction centers could be used to determine key chemical properties of the special pair was first introduced by Allen, Williams, Lubitz, and co-workers.[4,5] They obtained data for the M160 series of mutants, interpreting the data using a model that assumed that the only effect of mutation at the M160 site was modulation of the electric field felt by P_M and hence the energy gap E_0. They also ignored the reorganization energy λ^A, in effect adopting model E from Figure 1. We improved this analysis,[23] adding in addition the effects of the reorganization energy λ^A through adoption of model A, and adding a correction for the (minor) influence of the M160 mutation on the energy levels of P_L. Subsequently, Müh et al.[6] enhanced this theory and applied it to an expanded data set, examining in addition L131-series mutants as well as the M160-series mutants built on the wild-type+LH(L131) mutation and the L131-series mutants built on the wild-type+LH(M160). This resulted in considerable improvement in the quality of the analysis, but unique values for all of the key parameters still could not be extracted. Most recently, Johnson et al.[7] introduced two new series of mutants involving L135 and M164 variations, which introduced the observed value of the hole-transfer absorption energy into the analysis, allowing a unique solution to be obtained.

The basic assumption used by Allen and co-workers in their analysis of the properties of mutant reaction centers is that mutation affects only the in situ ionization energies U_M and U_L of the hypothetically charge-localized halves of the special pair,

from which the most important modulation is that of the energy difference

$$E_0 = U_M - U_L \tag{1}$$

In section 2, we examine the individual process through which this modulation occurs by calculating the changes in midpoint-potential E_m, charge densities ρ_L and ρ_M, and average hole-transfer transition energies $h\nu_{av}$ expected for mutations that modify only E_0. In section 3, we convolve this analysis slightly by allowing the mutations to individually modify both U_M and U_L, leading to the simulation of the observed midpoint potential as a function of charge density for the available mutant series. The correlation between hole-transfer electronic absorption energy and charge density is predicted in section 4 and compared to experiment, while in section 5 an a priori prediction of the observed electroabsorption Stark spectrum is presented. Central to all previous analyses of midpoint-potential and charge-density data is the use of the Born−Oppenheimer adiabatic approximation to the full nonadiabatic problem.[6,23,31] While the strengths and weaknesses of this approach are discussed in detail in sections 2−4, rigorous treatment is reserved for section 6 where previously obtained relationships[6,23,31] are simplified and extended to include, for the first time, the effects of symmetric modes. These formulas are particularly apt for general intervalence transfer problems in chemistry and biochemistry, for which control of E_0 can be systematically exerted by external modifications of say protein or ligand environments.

2. The Effect of the Redox Asymmetry E_0 on Molecular Properties

Depicted in Figure 2 are the change in midpoint potential from that for a localized oxidation of P_L, $E_m - E_m^L$, the charge density on P_L, ρ_L, and the average electronic transition energy $h\nu_{av}$, all shown as a function of the redox asymmetry E_0. These curves are calculated first from our full four-state model[31] of the special-pair radical cation of *Rb. sphaeroides*, varying only E_0 from its optimized value of 0.069 eV. Also shown are results obtained by eliminating contributions from the two SHOMO → HOMO-type states (reducing the model to just two electronic states), by also neglecting symmetric-mode contributions, and by the adiabatic approximation to the two-state no-symmetric-mode case. The adiabatic equations for the two-state model including symmetric-mode contributions are described later in section 6; the displayed curves are obtained by setting the symmetric-mode reorganization energy λ^S to zero. In the figure, E_0 spans the range from −0.05 to 0.2 eV, a range wide enough to include most species that have been produced by site-directed mutagenesis; for example, $E_0 = -0.011$ eV for LH(L131) and 0.168 eV for LH(M160), two mutations that have relatively large effects (see Table 1). Also provided in Figure 2 are insets showing the deviation of the calculated properties from that predicted by the two-state no-symmetric-mode adiabatic model over the wider range of $0 \leq E_0 \leq 1.2$ eV.

At large positive values of E_0, the calculated midpoint potentials E_m (Figure 2A) very slowly approach their asymptotic fully localized value E_m^L, while at large negative values, the midpoint potential decreases linearly with E_0 as then oxidation occurs from P_M rather than P_L. Eliminating the SHOMO → HOMO states results in a systematic increase in the midpoint potential of 0.003 eV, while the symmetric vibrational modes
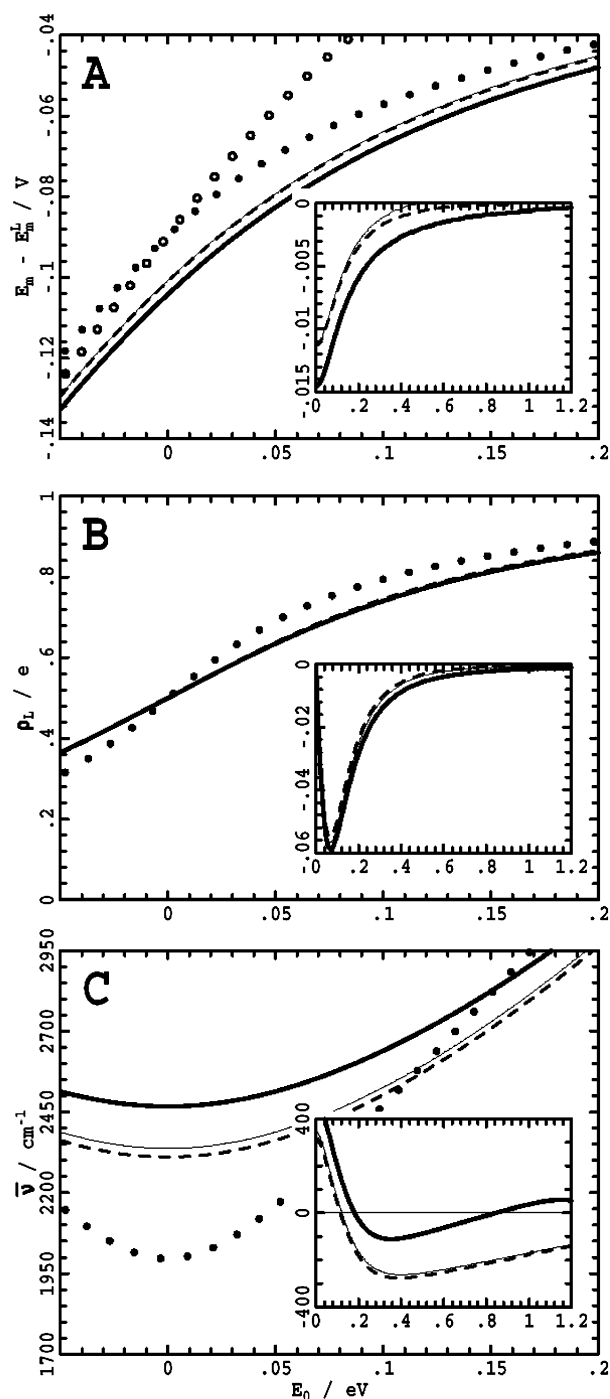
Figure 2. Calculated midpoint potentials (A), charge localizations (B), and hole-transfer average excitation frequencies (C) obtained from various vibronic-coupling models by varying only the redox asymmetry E_0: thick line, full four-state model; thin line, two-state model; dashed line, two-state model without symmetric vibrations; closed-circle line, adiabatic two-state model; open-circle line, alternate adiabatic model for E_m with $E_0 < 0$ akin to eq 26. The insets show only the differences between the nonadiabatic results and the analytical expressions.

Table 1. Observed Properties of Mutant Reaction Centers of *Rb. sphaeroides*[a]

mutant	E_m/V	ρ_L/ρ_M	ρ_L/e	E_0/eV	ν_{av}/cm^{-1}
LH(L131)+LN(M160)	0.591	0.82	0.45	−0.018	
LH(L131)+LS(M160)	0.584	0.83	0.45	−0.017	
LH(L131)	0.578	0.89	0.47	−0.010	2550
LE(L131)	0.555	1.00	0.50	0.000	
LH(L131)+LD(M160)	0.606	1.10	0.52	0.009	
LD(L131)	0.544	1.37	0.58	0.028	
LQ(L131)	0.551	1.43	0.59	0.032	
LS(L131)	0.535	1.49	0.60	0.036	
LH(L131)+LQ(M160)	0.619	1.51	0.60	0.037	
LN(L131)	0.535	1.57	0.61	0.041	
LH(L131)+LE(M160)	0.623	1.86	0.65	0.056	
LK(M160)	0.511	1.92	0.66	0.060	
wild-type	0.503	2.11	0.68	0.069	2560
LS(M160)	0.514	2.11	0.68	0.069	
LH(L131)+LH(M160)	0.621	2.21	0.69	0.073	2610
LN(M160)	0.527	2.31	0.70	0.078	
LD(M160)	0.539	2.77	0.73	0.097	
LE(L131)+LH(M160)	0.615	2.99	0.75	0.105	
LD(L131)+LH(M160)	0.600	3.20	0.76	0.113	
LQ(L131)+LH(M160)	0.600	3.23	0.76	0.114	
LQ(M160)	0.544	3.65	0.78	0.128	
LE(M160)	0.546	3.82	0.79	0.134	
LN(L131)+LH(M160)	0.583	3.89	0.80	0.136	
LS(L131)+LH(M160)	0.594	4.08	0.80	0.142	
LY(M160)	0.558	4.71	0.82	0.161	
LH(M160)	0.563	4.94	0.83	0.168	2780
RE(M164)	0.471	1.29	0.56	0.023	2450
RL(M164)	0.487	1.55	0.61	0.039	
RL(L135)	0.483	2.90	0.74	0.102	2450
RE(L135)	0.466	3.14	0.76	0.111	

[a] Values of the midpoint-potential E_m and spin density ratio ρ_L/ρ_M are from refs 4, 6, 7, 56, and 58; the redox asymmetry E_0 is determined from ρ_L using the four-state-model[31] correlation from Figure 2A; the average hole-transfer absorption energy ν_{av} is obtained using eq 2 to analyze the spectra from refs 7 and 9.

appropriate for a particular region depending on the sign of E_0, and results from both equations are shown in Figure 2A. Around $E_0 = 0$, quantum-mechanical tunneling between the vibrational energy levels in each localized well dominates the midpoint potential, an effect that is not included in the adiabatic approach. In this region, fluctuations in E_0 may also act to induce localization on short time scales, and hence different time-scale experiments may return different measures of properties such as the degree of charge localization.

The charge density localized on P_L, ρ_L (Figure 2B), is an odd function of E_0 that tends asymptotically to reflect complete charge localization on one of the halves of the special pair. Most interestingly, the asymptotic limits are again reached very slowly. Heterodimer mutants[48,49] such as HL(M202) that cause a bacteriochlorophyll in the special pair to be replaced by a bacteriopheophytin are anticipated to produce some of the largest accessible values of E_0 because the observed increase of E_0 in solution for the monomers is[50] 0.20 eV. Due to the slow asymptotic convergence shown in Figure 2B, 5−10% of the spin density is still anticipated to delocalize onto the bacteriopheophytin, however. Experimentally,[49] some such spin density is apparent but is too small to be readily quantified: if obtained, it would provide important information concerning the electronic coupling J in the heterodimer.

have almost no influence. The adiabatic approximation slightly underestimates the potential at large E_0 and significantly overestimates it at small and negative values, with the crossover point of minimal error occurring fortuitously in the most important region, that characteristic of the wild-type near $E_0 = 0.068$ eV. As discussed later, adiabatic theory actually leads to two different solutions (eq 25 and 26), each of which is

(48) Bylina, E. J.; Kolaczkowski, S. V.; Norris, J. R.; Youvan, D. C. *Biochemistry* **1990**, *29*, 6203.
(49) Huber, M.; Isaacson, R. A.; Abresch, E. C.; Gaul, D.; Schenck, C. C.; Feher, G. *Biochim. Piophys. Acta* **1996**, *1273*, 108.
(50) Fajer, J.; Davis, M. S.; Brune, D. C.; Spaulding, L.; Borg, D.; Forman, A. *Brookhaven Symp. Biol.* **1976**, *28*, 74.

The spin densities predicted after exclusion of the SHOMO → HOMO states and/or the symmetric modes are insignificantly different from those predicted by the full model. The adiabatic approximation reaches its maximum error of $0.06e$ in the region of the wild-type, and hence application of analytical formula for the charge density is quite hazardous. For *Rb. sphaeroides*, however, the adiabatic surface has only one minimum, and hence the correct result of $\rho_L = 0.5$ at $E_0 = 0$ is obtained. The curve analogous to that of Figure 2B for PS-I systems will appear quite different, however, because the adiabatic potential for these is most likely to have two minima. Different adiabatic equations will then apply depending on the sign of E_0; rather than meeting at $E_0 = 0$, these curves will diverge and give large errors in this region.

Calculated electronic hole-transfer average absorption energies $h\nu_{av}$ are shown in Figure 2C. If the initial and final potential-energy surfaces are harmonic and the Condon[51,52] approximation of coordinate-independent transition probability holds, then this averaged frequency corresponds[53,54] to the vertical energy difference between the ground and excited states evaluated at the equilibrium geometry of the ground state, the so-called vertical excitation energy. Because of the vibronic couplings from the hole-transfer state to both the ground state and the SHOMO → HOMO state, the Condon approximation is not valid, and hence the connection between $h\nu_{av}$ and the vertical excitation energy is blurred. However, for arbitrary potential-energy surfaces and linear vibronic coupling, the reflection approximation to spectroscopic band shapes may be evoked to give the same result.[55] Although not explicitly stated in earlier derivations,[53–55] this later result only applies for nonoverlapping electronic transitions. In the present application, it is practical to separate out the phase-phonon intensity from the hole-transfer band but not that of the SHOMO → HOMO state, and hence we define the average absorption energy as

$$\nu_{av} = \frac{\int_{\nu_{min}}^{\nu_{max}} A(\nu)\, d\nu}{\int_{\nu_{min}}^{\nu_{max}} \frac{A(\nu)}{\nu}\, d\nu} \tag{2}$$

where $A(\nu)$ is the observed absorption strength as a function of frequency, and ν_{min} and ν_{max} select the region of interest. This region is unambiguously $\nu_{min} = 1650$ cm^{-1} and $\nu_{max} = 5000$ cm^{-1} for analysis of calculated spectra. However, the observed SHOMO → HOMO band (at ca. 2200 cm^{-1}) overlaps the vibrational structure somewhat, other electronic transitions may be present above $\nu = 5000$ cm^{-1}, and in many cases the experimental absorption above 3500 cm^{-1} is not necessarily well depicted; we thus choose $\nu_{min} = 1650$ cm^{-1} and $\nu_{max} = 4000$ cm^{-1} for the analysis of experimental data, although variations in these limits are significant.

If ν_{av} is large as compared to the width of the band and the band shape A/ν as a function of ν is Gaussian in nature, then ν_{av} may be approximated from the wavelength of the maximum absorption obtained in the usual way from the absorption as a function of wavelength. All of these assumptions are violated for the case of hole-transfer absorption, however, as for this spectroscopic class the band shape is highly variable[2] and never Gaussian, while the bandwidth is usually large as compared to the average frequency. Hence, quantitative analysis of the absorption energy must proceed via explicit evaluation of ν_{av}, despite the requirement of high-quality spectra in both the low-frequency and the high-frequency tail regions.

The calculated average hole-transfer transition energies display a minimum at, and are symmetric about, $E_0 = 0$; in the asymptotic region of large E_0, ν_{av} increases in proportion to E_0. The derivative $d\nu_{av}/dE_0$ is usually called the Stark tuning rate and is a constant for most molecular spectroscopic systems. Figure 2C shows that this is not the case for hole-transfer bands, however, as the tuning rate changes dramatically for small $|E_0|$. The calculated average absorption frequency for the wild-type ($E_0 = 0.0688$ eV) is 2550 cm^{-1} (from the observed spectrum,[10] this value is 2560 cm^{-1}), whereas the minimum attainable value of ν_{av} is only 90 cm^{-1} lower. It is hence clear that the shoulder observed near 2200 cm^{-1} in the absorption spectrum that we interpret[2] as a SHOMO → HOMO transition cannot arise from a Stark effect of the main hole-transfer band induced by some site variation that affects only the external electric field felt by the special pair.

As shown in Figure 2C, neglect of the presence of the SHOMO → HOMO transition from the calculated spectra has a profound effect on the average hole-transfer absorption energy. Within the region of greatest interest, ν_{av} is increased by 160 cm^{-1} as a result of the interaction. This change results from the partial cancellation of two terms, one which pushes the hole-transfer band to higher energy, and another which reduces ν_{av} due to the intensification of the hole-transfer band itself. Symmetric modes are seen to have only a minor influence on ν_{av}, however.

For large values of E_0, the adiabatic approximation to ν_{av} overestimates the transition energy, although extremely slow convergence toward the full nonadiabatic value is evident from Figure 2C. However, for $|E_0| < 0.15$ eV (i.e., the range appropriate to the wild-type and most mutants of *Rb. sphaeroides*), ν_{av} is underestimated by up to 300 cm^{-1} as compared to the two-state nonadiabatic predictions and up to 500 cm^{-1} (or 20%) as compared to the full four-state simulated results. The serious failure of the adiabatic approximation in this region has been noted previously,[46] and, as a result, values of key parameters such as $|J|$ deduced using adiabatic theories are significant in error. As an example, the value of $|J|$ deduced by Johnson et al.[7] of 0.155 eV is significantly larger than the value of 0.126 ± 0.002 eV obtained from full nonadiabatic simulation,[31] a value that is shown in the next section to adequately describe their raw experimental data.

3. The Correlation between the Midpoint Potential and the Charge Density for Mutant Reaction Centers

A procedure for estimating key properties of the special-pair radical cation based upon the correlation between observed midpoint potentials and observed spin densities was introduced by Allen and co-workers[4,5] and subsequently developed.[6,7,23] The interpretation of this correlation is based on the two-state adiabatic theory. While past treatments have neglected the contributions from symmetric modes and in the previous section

(51) Condon, E. U. *Phys. Rev.* **1928**, *32*, 858.
(52) Lax, M. *J. Chem. Phys.* **1952**, *20*, 1752.
(53) Richardson, W. B.; Lin, S. H.; Evans, D. L. *J. Chem. Soc., Faraday Trans. 2* **1982**, *78*, 1.
(54) Kubo, R. *Phys. Rev.* **1952**, *86*, 929.
(55) Sulzer, P.; Wieland, K. *Helv. Phys. Acta* **1952**, *25*, 653.

we justified this procedure, a full derivation of the appropriate equations including the effects of symmetric modes is given in section 6 (see in particular eqs 25,26). However, the errors demonstrated in Figure 2 for the adiabatic approach are so large that they indicate that quantitatively accurate values of the key parameters J, λ^A, and E_0 cannot be obtained.

Interpretation of the experimental data also relies on the assumption that the only effect of site-directed mutagenesis of the surrounding protein is to shift the energy levels of the two halves of the special pair. While the difference between the energy-level shifts between the two bacteriochlorophylls changes the redox asymmetry E_0 (see Figure 2A, and eqs 25,26), there is also a change in the mean energy of P_L^+ and P_M^+ that contributes to the observed midpoint potential. In early studies[23] based on the M160 series mutants, it was clear that inclusion of the direct effect was necessary but there was insufficient experimental data to permit quantitative analysis. Subsequently,[6] the available experimental data set has been greatly expanded through examination of the L131 series mutants as well as the LH(M160)+L131 and LH(L131)+M160 series of double mutants. As the M160 and L131 residues are nearly symmetrically related on each side of the reaction center, it is assumed that the relative effects of the mutation on the near and far halves of the special pair are the same. For some properties, the same L131 and M160 site mutations can have quite different manifestations due to the subtle asymmetries present,[22] but such effects are not expected to apply for the properties of interest herein. Assuming also that the effects of multiple mutations are additive, the effects of mutation on the energy levels of each half of the special pair can then be expressed in terms of the redox asymmetry E_0 and one additional parameter[46] η as $\Delta U_L =$

M160: $\eta \Delta E_0$

L131: $-(1 + \eta)\Delta E_0$

LH(L131)+M160: $\eta[\Delta E_0 - \Delta E_0^{LH(L131)}] -$

                 $(1 + \eta)\Delta E_0^{LH(L131)}$

LH(M160)+L131: $-(1 + \eta)[\Delta E_0 - \Delta E_0^{LH(M160)}] +$

                 $\eta[\Delta E_0 - \Delta E_0^{LH(M160)}]$ (3)

and $\Delta U_M =$

M160: $(1 + \eta)\Delta E_0$

L131: $-\eta \Delta E_0$

LH(L131)+M160: $(1 + \eta)[\Delta E_0 - \Delta E_0^{LH(L131)}] -$

                 $\eta \Delta E_0^{LH(L131)}$

LH(M160)+L131: $-\eta[\Delta E_0 - \Delta E_0^{LH(M160)}] +$

                 $(1 + \eta)\Delta E_0^{LH(M160)}$ (4)

where ΔE_0, ΔU_L, and ΔU_M are the change in the redox asymmetry and absolute energy levels of P_L^+ and P_M^+ from the values in the wild-type, respectively, and $\Delta E^{LH(L131)}$, etc., are the appropriate values for the single mutant. Note that, for all series, $\Delta E_0 = \Delta U_M - \Delta U_L$. The analogous equations used in the early studies on just the M160 series[4,5,23] in which the
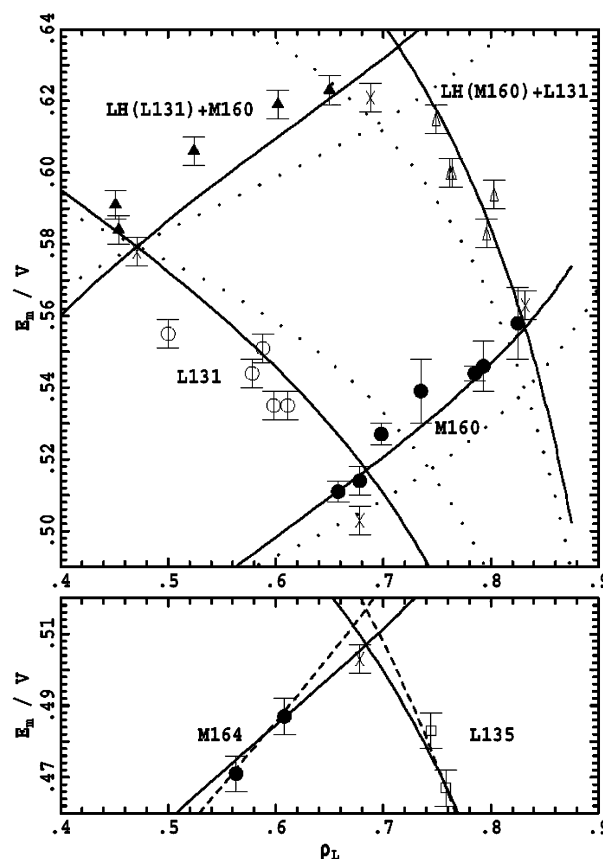
Figure 3. Midpoint-potential E_m as a function of charge delocalization ρ_L on the P_L half of the special-pair radical cation for *Rb. sphaeroides* wild-type and mutant reaction centers (see Table 1), as compared to the correlations expected from our four-state model for different mutant series (—, $\eta = 0.18$ (top) and 0.28 (bottom); – – –, $\eta = 0.54$; •••, adiabatic approximation to $\eta = 0.18$ from eq 25). The wild-type, LH(M160), LH(L131), and LH(L131)+LH(M160) mutants each belong to two mutant series and are indicated by ×, while △, ▲, ■, □, ●, and ○ identify individual members of the same series.

mutation was assumed not to affect P_L correspond to the case with $\eta = 0$. In the more recent study[6] on all four series. it was estimated that $\eta \approx 0.2$, consistent (see later) with the relative geometries of the cofactors and the M160 and L131 residues. Note that these later workers[6] have adopted a slightly different definition of η than our original definition[23] that we again use herein, replacing η with $\eta/(1 + \eta)$. The differences are small for small η.

The observed[4,6,56] midpoint-potentials E_m as a function of charge densities (approximated[6,57] from the observed spin densities) are given in Table 1 and shown graphically in Figure 3 for all 26 mutant species that have been constructed belonging to these series. Note that the wild-type, LH(L131), LH(M160), and LH(L131)+LH(M160) mutants each belong to two different series as explicitly indicated. Shown also in the figure are curves for each mutant series, indicating the correlation predicted using our four-state full vibronic-coupling model. To apply this model, two additional adjustable parameters arise: the midpoint potential of an isolated P_L residue E_m^L and the value of η. Fitting these to the experimental data, we obtain $\eta = 0.18$, the same as earlier estimates,[6] with the root-mean-square (RMS) error in

(56) Rautter, J.; Lendzian, F.; Schulz, C.; Fetsch, A.; Kuhn, M.; Lubitz, W.; Lin, X.; Williams, J. C.; Allen, J. P. *Biochemistry* **1995**, *34*, 8130.
(57) Reimers, J. R.; Hutter, M. C.; Hughes, J. M.; Hush, N. S. *Int. J. Quantum Chem.* **2000**, *80*, 1224.

Table 2. Optimized Values of η for Various Series of Mutants of *Rb. sphaeroides* and Their Interpretation in Terms of the Relative Distance x of the Mutant Site to the Nearest and Furthest Halves of the Special Pair, As Compared to Geometrical Estimates of x

| | | | | | x | |
| | | | at | at | to cofactor | to cofactor |
series	η	x^n	$n = 1$	$n = 2$	center	edge
M160, L131	0.18	0.15	0.15	0.39	0.61	0.32
M164, L135	0.28	0.22	0.22	0.47	0.65	0.51
M164, L135	0.54	0.35	0.35	0.59	0.65	0.51

this fit being 0.0088 V, which is approximately double the typical experimental error in determining E_m. Figure 3 indicates that the experimental data show good semiquantitative agreement with the predicted curves. While it is possible that reoptimization of the parameters in our four-state model could reduce the difference between the observed and predicted correlation, it is apparent that experimental variations occur that cannot all be quantitatively reproduced by such a procedure. We see that, to some small degree, breakdown occurs of the primary assumption used in the data analysis that the only effect of mutation is to modify the local energy levels. Indeed, such a result is expected as the mutations necessitate significant changes of the protein background to form their observed hydrogen-bonded structures.[22] Hence, it is not clear that reoptimization would lead to a physically more realistic description of the properties of the system.

The LH(L131) and LH(M160) mutations have also been combined with the heterodimer mutation HL(M202).[56] These species allow for an independent verification of the conclusions drawn from Figure 3. While quantitative analysis requires more precise knowledge of the effects of the heterodimer mutation on E_0 and spin distributions than is currently available, progress can be made by assuming $E_0 = \infty$ so that $\rho_L = 1$. In this case, η can be expressed directly as

$$\eta = \frac{E_m^{\text{HL(M202)+LH(M160)}} - E_m^{\text{HL(M202)}}}{E_m^{\text{HL(M202)+LH(L131)}} - E_m^{\text{HL(M202)+LH(M160)}}} \quad (5)$$

which evaluates to $\eta = 0.15 \pm 0.09$ using the measured[56] midpoint potentials. This value agrees with the value of 0.18 obtained more precisely from the extensive data set as shown in Figure 3. It demonstrates the validity of the basic chemical model embodied in eqs 3 and 4.

The appropriate value of η can also be estimated by considering the geometrical relationships between the residues and the cofactors. If the ratio of the distance between the (approximate center of the) mutation site and its nearest special-pair cofactor to that of its furthest cofactor is x, and if the protein environment can be modeled as a uniform dielectric material, then from classical electrostatics

$$x^n = \frac{\eta}{1 + \eta} \quad (6)$$

where n is the power in the appropriate force-law; that is, $n = 1$ if the mutation involves a change in the charge of the mutated residue, $n = 2$ if only the dipole moment of the residue changes, etc. The optimized value of η is given in Table 2, along with values of x obtained assuming either $n = 1$ or $n = 2$ and values obtained from the optimized structures of the mutants[22] for the

distance both to the edge and to the center of the cofactors. For the M160 and L131 mutants and double mutants, only changes in dipole are involved; the value of x obtained at $n = 2$, 0.39, is within the range of values of $0.32 < x < 0.61$ anticipated from the edge and center distances, respectively, while the $n = 1$ value of 0.15 is outside the expected range. Note, however, that these estimates are based on the assumption of a uniform dielectric background, an assumption that has been questioned,[58] and we shall subsequently consider the likely consequences of this in detail.

Johnson et al.[7] have constructed alternate series of mutants based on site-directed mutagenesis at the symmetrically related M164 and L135 positions. The available experimental data[7] are shown in Figure 3; this comprises the wild-type and four mutants: RE(M164), RL(M164), RL(L135), and RE(L135). As these mutants should depict the same value of E_m^L as for the L131 and M160 mutants, we first freeze this parameter at the previously optimized value and optimized $\eta = 0.54$ to fit the experimental data with a RMS error of 0.0057 V. However, from examination of the results in Figure 3, it is clear that replacement of the leucene at sites L131 or M160 with any hydrogen-bonding residue introduces a jump of 0.010 V in the midpoint potential. The mechanism leading to this jump is unknown and could arise from specific hydrogen-bonding modulation of either the charge-localized midpoint potentials, the electronic coupling, or the reorganization energy; in our fit to the experimental data, the simplest approach of including this within E_m^L is taken. Optimization of both E_m^L and η results in the RMS error falling to 0.0036 V and $\eta = 0.28$. Both fits to the experimental data are depicted in Figure 3 and in Table 2.

From the geometrical relationships of the sites of the M164 and L135 mutations to the special pair, we expect distances ratios within the range $0.51 < x < 0.65$, as indicated in Table 2. From the optimized values of η of 0.28−0.54, for a dipolar interaction with $n = 2$ we determine $x = 0.47$−0.59, respectively, in good agreement with the geometrical estimate. However, assuming that the mutations involve a change in residue charge ($n = 1$) leads to significant underestimation of x as 0.22−0.35, respectively. As the M164 and L135 sites form part of the hydrophilic/hydrophobic boundary within the protein, it is possible, and commonly assumed,[7,58] that ionizable residues in these sites are indeed ionized. Our analysis naively suggests that they are not ionized, however, but only affect the special pair through the differing dipole moments of the residues. This analysis is based on the assumption of a uniform dielectric material; in an alternative approach, the redox midpoint potentials of these mutants have been interpreted in terms of ionized residues using a strongly distance-dependent dielectric function.[58] Such a nonuniform dielectric function is appropriate if unspecified counterions are present in the vicinity of the residues, an effect that causes the electrostatic interactions to appear, at long distance, to be of dipolar form ($n = 2$) rather than of ionic form ($n = 1$). Hence, we see that, while the observed value of η contains important information concerning protein structure and function, authoritative analysis is difficult to perform and much more experimental work is required in this area.

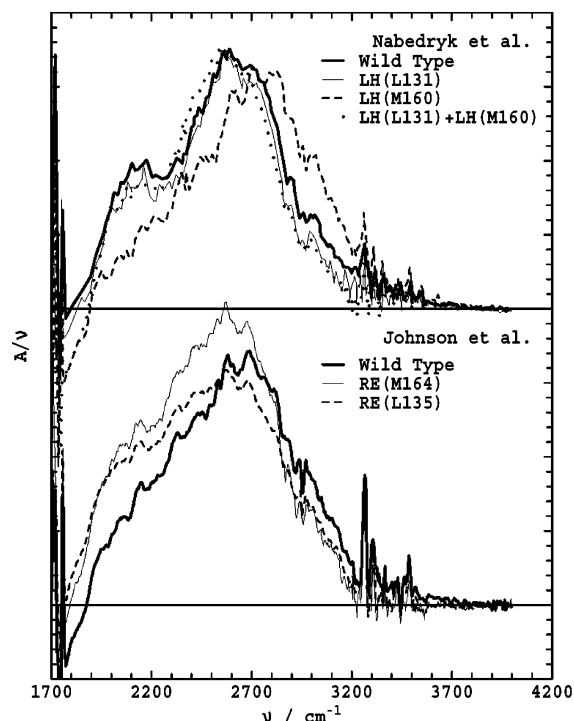(58) Johnson, E. T.; Parson, W. W. *Biochemistry* **2002**, *41*, 6483.

Figure 4. Observed hole-transfer absorption spectra shown as A/ν as a function of ν to give a realistic impression of the relative importance of the low-frequency and high-frequency regions of the spectrum, taken from the studies of Nabedryk et al.[9] for the wild-type, LH(L131), LH(M160), and LH(L131)+LH(M160) mutants, and Johnson et al.[7] (dry, cooled in the dark) for the wild-type, RE(L135), and RE(M164) mutants.

4. The Correlation between the Intervalence Hole-Transfer Excitation Energy and the Charge Density for Mutant Reaction Centers

The observed spectra[7,9] for the wild-type and available mutants of *Rb. sphaeroides* are shown in Figure 4, and the average hole-transfer electronic absorption energies ν_{av} evaluated from these using eq 2 are given in Table 1. The correlation between these frequencies and the observed[4,6,56,58] charge densities ρ_L is shown in Figure 5, along with the correlation predicted based on our four-state model for the special-pair radical cation. Qualitative agreement is found between the predicted correlation and the data for the wild-type, RE(M164), LH(L131), and LH(L131)+LH(M160) mutants, but ν_{av} for the LH(M160) and especially RE(L135) mutants are much lower than expected. One aspect of the relatively poor agreement between prediction and experiment is the difficulties noted in section 2 concerning reliable determination of ν_{av} from the experimental spectra. Sample preparation is also an issue,[7] and we analyze spectra of partially dried reaction centers that were cooled to cryogenic temperatures in the dark. The spectra shown in Figure 4 were taken from two sources, the wild-type, LH(L131), LH(M160), and LH(L131)+LH(M160) from Nabedryk et al.,[9] while the spectra for wild-type (again), RE(M164), and RE(L135) were taken from Johnson et al.[7] To check that these sets of spectra are comparable, we also evaluated ν_{av} for the wild-type from the spectrum of Johnson et al., obtaining 2620 cm^{-1} as compared to 2560 cm^{-1} from the spectrum of Nabedryk et al. This difference is of the order of the errors associated with the analysis of any particular spectrum, and hence differing methods of sample prep-
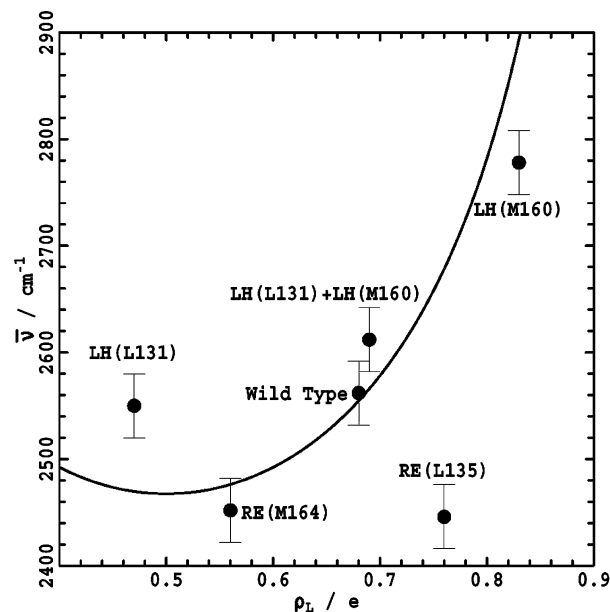
Figure 5. Correlation between the observed average hole-transfer absorption energy ν_{av} and the observed charge localization ρ_L on the P_L half of the special-pair radical cation for *Rb. sphaeroides* wild-type and mutant reaction centers (see Table 1), as compared to that expected from our four-state model for different mutant series (solid line). The expected correlation is based on the assumption that mutation affects only E_0.

aration or optical configuration appear not to be especially significant.

The poor correlation between predicted and experimental results appears to be due to breakdown of the assumption that the only effect of mutation is the change in the redox asymmetry E_0. From the observed spectra shown in Figure 4, it is clear[59] that the 2200 cm^{-1} shoulder adjusts independently of the modulation in frequency of the hole-transfer band and hence mutation clearly affects also the energy of the SHOMO → HOMO state. Independent modulation of E_0 and the SHOMO → HOMO energy with mutation is possible as quite different changes in dipole moment can accompany these transitions as they are of fundamentally different natures. Because of the strong vibronic coupling between the SHOMO → HOMO and hole-transfer states, it is only possible to consider the average frequency ν_{av} of both bands combined, and hence the neglect of the effect of mutation on the SHOMO → HOMO energy has profound consequences. Inspection of the original spectra[7] suggests that the SHOMO → HOMO band may be lowered by ca. 100–200 cm^{-1} in RE(M164) and RE(L135), an effect that would significantly modify ν_{av}.

5. Prediction of the Electroabsorption Stark Spectrum of *Rb. sphaeroides*

In the previous sections, the properties of the special-pair radical cation of *Rb. sphaeroides* were examined as modulated using site-directed mutagenesis to control the electric field across the special pair. It is possible to control the electric field and hence E_0 directly through the application of an external electric field. Treynor, Andrews, and Boxer[11] have measured this electroabsorption Stark spectrum for *Rb. Sphaeroides*, and their spectrum is shown in Figure 5 along with our predicted spectrum. The applied electric field interacts with the localized

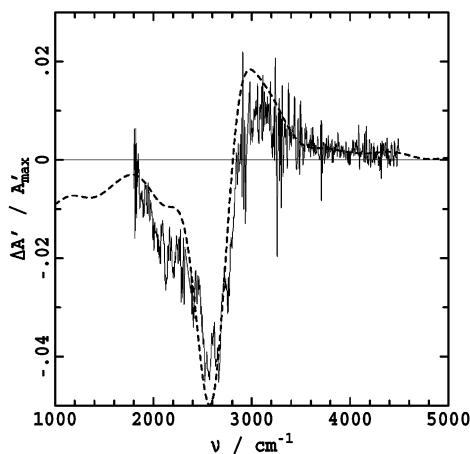(59) Reimers, J. R.; Hutter, M. C.; Hush, N. S. *Photosynth. Res.* **1998**, *55*, 163.

Figure 6. The observed electroabsorption Stark spectrum of Treynor, Andrews, and Boxer[11] (—) for the wild-type of *Rb. sphaeroides* as compared to that predicted by our four-state model (− − −); both are scaled to an applied electric field strength of 1 MV cm^{-1} and depict $A' = A/\nu$.

dipole moments and polarizabilities of the two halves of the special pair. We have shown[43,60] that for intervalence absorptions these quantities are dominated by the contributions arising from within the ground and charge-transfer states themselves, allowing the isotropically averaged electroabsorption Stark spectrum to be expressed as

$$\Delta A'(\nu) = A'_F(\nu) - A'(\nu) = A'(\nu; E_0 - \Delta E_0) - 2A'(\nu; E_0) + A'(\nu; E_0 + \Delta E_0) \quad (7)$$

where

$$A'(\nu) = \frac{A(\nu)}{\nu} \quad (8)$$

is the absorption band profile, $\Delta A'$ is the change in absorption profile for an applied field of magnitude F, A'_F is the absorption profile at the applied field strength, $A'(\nu; E_0)$ is the calculated absorption profile from our four-state model evaluated with redox asymmetry E_0, and ΔE_0 is the field-induced maximal change in redox asymmetry

$$\Delta E_0 = fF\Delta\mu^L[R(\chi)]^{1/2} \quad (9)$$

where f is the local field correction factor, $R(\chi)$ is a geometrical factor[34,43,60] representing the experimental alignment of the optical and electrostatic fields, and $\Delta\mu^L$ is the magnitude of the change in dipole moment associated with the excitation from fully localized $P_L^+P_M$ to $P_LP_M^+$. Treynor et al.[11] have estimated the local field correction factor as $f = 1.15 \pm 0.15$ and, at the configuration used in their experiments, $R(\chi) = 1/5$. All results shown in Figure 6 are rescaled to an applied field strength of $F = 1$ MV cm^{-1} and also normalized by the maximum absorption A'_{max}. Note that presenting the spectra in terms of $A' = A/\nu$ provides a visual impression that correctly balances the importance of the low-frequency and high-frequency components of the spectra.

One parameter appears in this expression that is in addition to those already found in our four-state model of the special-pair radical cation, and that is $\Delta\mu^L$. In principle,[14,60] this quantity

(60) Reimers, J. R.; Hush, N. S. *J. Phys. Chem.* **1991**, *95*, 9773.

can be related to the electronic transition moment M that does appear in the model, but for *Rb. sphaeroides*, configuration interaction effects with states outside the four explicitly considered break this nexus.[45,46] Previously,[26] many of the parameters in our model were evaluated using density-functional theory, and from the results of those calculations it is possible to estimate $\Delta\mu^L$. To do this, we take the Mulliken charges evaluated at the B3LYP/3-21G optimized structures for the neutral and ionized monomers and place them on the atoms from the B3LYP/3-21G optimized structure of the special pair. In this fashion, charge distributions for the hypothetical fully charge-localized $P_L^+P_M$ and $P_LP_M^+$ states are obtained, and hence $\Delta\mu^L$ is evaluated[26] to be 6.527 e Å = 31.3 D. This allows the a priori estimation of the electroabsorption Stark spectrum.

The observed and calculated spectra shown in Figure 6 are in good agreement with each other. The form of the electro-absorption response for charge-transfer transitions is intermediate between the classical second-derivative (with two nodes) and first-derivative (with one node) Liptay responses;[43] it can thus change dramatically in appearance with variation of the interactions within the charge-transfer system. For *Rb. sphaeroides*, both the calculated and the predicted spectra show a single node appearing at similar locations. Further, the overall amplitude of the spectra agrees to within the experimental uncertainties in estimating the local field correction factor. Finally, the calculated and observed electroabsorption of the 2200 cm^{-1} shoulder are in qualitative agreement with each other. This part of the calculated spectrum is very sensitive to the treatment of the SHOMO → HOMO band, and it provides strong evidence to support the band assignment. In principle, dramatic variation of the Stark spectrum in this region could be anticipated, with the appearance of either one or two additional nodes in this region. Indeed, such occurrences are common in electro-absorption spectra of inorganic charge-transfer complexes,[34] making this technique a very revealing one for weak shoulder transitions. Only a remarkable coincidence of properties could enable a transition involving a chromophore other than the special pair to give rise to a signal such as that observed.

6. Analytical Solution to the Two-State Model Using the Born−Oppenheimer Adiabatic Approximation

Our full vibronic-coupling model[2,26,31,46] for the special-pair radical cation involves four electronic states; neglecting the two states involving SHOMO → HOMO excitation, the localized and delocalized diabatic Hamiltonians $\mathbf{H_L}$ and $\mathbf{H_D}$, respectively, for the system[31] can be expressed in terms of just the ground electronic state (GS) and hole-transfer electronic state (HT) using n' symmetric dimensionless normal vibrational coordinates q'_i of frequency ν'_i and n'' antisymmetric dimensionless normal vibrational coordinates q''_j of frequency ν''_j as

$$\mathbf{H_L} = \begin{bmatrix} H_L^{GS \leftrightarrow GS} & H_L^{GS \leftrightarrow HT} \\ H_L^{GS \leftrightarrow HT} & H_L^{HT \leftrightarrow HT} \end{bmatrix} \quad \text{and}$$

$$\mathbf{H_D} = \begin{bmatrix} H_D^{GS \leftrightarrow GS} & H_D^{GS \leftrightarrow HT} \\ H_D^{GS \leftrightarrow HT} & H_D^{HT \leftrightarrow HT} \end{bmatrix} \quad (10)$$

where

$$H_D^{GS \leftrightarrow GS} = -J + \frac{1}{2}\sum_{j=1}^{n''} h\nu_j''[(\dot{q}_j'')^2 + (q_j'')^2] +$$

$$\frac{1}{2}\sum_{i=1}^{n'} h\nu_i'[(\dot{q}_i')^2 + (q_i' + \delta_i')^2]$$

$$H_D^{HT \leftrightarrow HT} = -J + \frac{1}{2}\sum_{j=1}^{n''} h\nu_j''[(\dot{q}_j'')^2 + (q_j'')^2] +$$

$$\frac{1}{2}\sum_{i=1}^{n'} h\nu_i'[(\dot{q}_i')^2 + (q_i' - \delta_i')^2]$$

$$H_D^{GS \leftrightarrow HT} = -\frac{E_0}{2} + \sum_{j=1}^{n''} \alpha_j'' q_j'' \tag{11}$$

and

$$H_L^{GS \leftrightarrow GS} = -\frac{E_0}{2} + \frac{\lambda^S - \lambda^A}{4} + \frac{1}{2}\sum_{j=1}^{n''} h\nu_j''[(\dot{q}_j'')^2 +$$

$$(q_j'' + \delta_j'')^2] + \frac{1}{2}\sum_{i=1}^{n'} h\nu_i'[(\dot{q}_i')^2 + (q_i')^2]$$

$$H_L^{HT \leftrightarrow HT} = \frac{E_0}{2} + \frac{\lambda^S - \lambda^A}{4} + \frac{1}{2}\sum_{j=1}^{n''} h\nu_j''[(\dot{q}_j'')^2 +$$

$$(q_j'' - \delta_j'')^2] + \frac{1}{2}\sum_{i=1}^{n'} h\nu_i'[(\dot{q}_i')^2 + (q_i')^2] \tag{12}$$

$$H_L^{GS \leftrightarrow HT} = J_{eff}$$

where J is the electronic coupling between the diabatic states, and J_{eff} is an effective electronic coupling[31,57] appropriate in the localized description that varies with the symmetric-mode coordinates

$$J_{eff} = J - \sum_{i=1}^{n'} h\nu_i \delta_i' q_i' \tag{13}$$

δ_i' values are the equilibrium displacements in the symmetric modes in the delocalized diabatic description, α'' likewise are the vibronic-coupling constants in the antisymmetric modes, δ_j'' is the effective displacement in the antisymmetric modes apt for the localized diabatic description (it is these displacements that comprise the generalized coordinate used for the abscissa in Figure 1)

$$\delta_j'' = \frac{\alpha_j''}{h\nu_j''} \tag{14}$$

and the antisymmetric-mode (A) and symmetric-mode (S) reorganization energies are defined by

$$\lambda^A = 2\sum_{j=1}^{n''} h\nu_j''(\delta_j'')^2 = 2\sum_{j=1}^{n''} \frac{(\alpha_j'')^2}{h\nu_j''}$$

$$\lambda^S = 2\sum_{i=1}^{n'} h\nu_i'(\delta_i')^2 \tag{15}$$

Note that the two diabatic Hamiltonians are related[31,46] by

rotation through 45°:

$$\mathbf{H_D} = \frac{1}{2}\begin{bmatrix} 1 & -1 \\ 1 & 1 \end{bmatrix} \mathbf{H_L} \begin{bmatrix} 1 & 1 \\ -1 & 1 \end{bmatrix} \tag{16}$$

while the projection operators which give the contribution of the localized state to an arbitrary admixed state are

$$\mathbf{P_L^{GS}} = \begin{bmatrix} 1 & 0 \\ 0 & 0 \end{bmatrix} \quad \text{and} \quad \mathbf{P_D^{GS}} = \frac{1}{2}\begin{bmatrix} 1 & 1 \\ 1 & 1 \end{bmatrix} \tag{17}$$

for the localized ground state and

$$\mathbf{P_L^{HT}} = \begin{bmatrix} 0 & 0 \\ 0 & 1 \end{bmatrix} \quad \text{and} \quad \mathbf{P_D^{HT}} = \frac{1}{2}\begin{bmatrix} 1 & -1 \\ -1 & 1 \end{bmatrix} \tag{18}$$

for the localized hole-transfer state.

Within the adiabatic approximation, most properties of significance depend only on the two reorganization energies and not upon the individual vibrational components. This arises because the minimum in the lower adiabatic potential-energy surface, obtained within the Born−Oppenheimer approximation[33] by diagonalizing equivilantly $\mathbf{H_L}$ or $\mathbf{H_D}$ parametrically as a function of the nuclear coordinates, takes the same form for each individual mode:[6,23,31]

$$q_{i,min}' = \delta_i'\left[1 - \frac{E_v^2}{(h\nu_{av})^2}\right]^{1/2} = -\delta_i'\left[1 - \frac{E_0^2}{(h\nu_{av} - \lambda^A)^2}\right]^{1/2} = -2\delta_i'(\rho_L\rho_M)^{1/2} \tag{19}$$

and

$$q_{j,min}'' = -\delta_j''\frac{E_v}{h\nu_{av}} = -\delta_j''\frac{E_0}{h\nu_{av} - \lambda^A} = -\delta_j''(\rho_L - \rho_M) \tag{20}$$

where E_v is the (signed) energy difference between the localized diabatic potential-energy surfaces for $P_L P_M^+$ and $P_L^+ P_M$ at the energy minimum, $h\nu_{av}$ is the corresponding (unsigned) adiabatic energy difference corresponding to the average excitation energy (eq 2), and ρ_L and $\rho_M = 1 - \rho_L$ are the corresponding spin densities on each localized half. When the coupling $2|J|$ or the redox asymmetry E_0 is large as compared to λ^A, the lower surface takes on a single minimum structure as depicted in Figure 1D and 1E. Indeed, Figure 1D shows the diabatic picture that is appropriate for *Rb. sphaeroides*, although it may not be so for PS-I and PS-II reaction centers. When λ^A dominates, the lower adiabatic surface has two minima, and in that case eq 20 depicts the minimum of lower energy, except for the case of $E_0 = 0$ as then the two minima have equal energy. The solution of this equation may become unstable as $E_0 = 0$, as in this case $h\nu_{av} - \lambda^A$ also becomes zero. In our previous treatment,[23] E_v was named "$E_0(q_{min})$" (the diabatic energy difference at the geometry of the adiabatic minimum); it is related to the redox asymmetry through[7]

$$E_v = E_0 + \lambda^A(\rho_L - \rho_M) \tag{21}$$

In deriving these equations, a key step is the identification of the charge density on each half at the adiabatic minimum from E_v and the effective coupling at this geometry given by

$$|J_{eff}| = |J|\frac{h\nu_{av}}{h\nu_{av} - \lambda^S} = |J| + \lambda^S(\rho_L\rho_M)^{1/2} = h\nu_{av}(\rho_L\rho_M)^{1/2} \tag{22}$$

and leads to, by analogy to eq 4 of ref 23,

$$\frac{E_v}{|J_{\text{eff}}|} = \left(\frac{\rho_L}{\rho_M}\right)^{1/2} - \left(\frac{\rho_M}{\rho_L}\right)^{1/2} \tag{23}$$

The adiabatic hole-transfer averaged excitation energy (also known as the vertical excitation energy) is also simply related to these quantities via

$$h\nu_{\text{av}} = (4J_{\text{eff}}^2 + E_v^2)^{1/2} \tag{24}$$

Finally, the midpoint-potential E_m of the dimer is obtained from the minimum energy of the lower adiabatic surface by analogy with eq 11 of ref 23. However, the intrinsic two-well nature of the localized diabatic description becomes explicitly manifest here in that different equations become appropriate in different regions: for $E_0 > 0$, we obtain

$$FE_m = U_L + (\lambda^A - \lambda^S)\rho_M^2 - |J|\left(\frac{\rho_M}{\rho_L}\right)^{1/2} + FC \tag{25}$$

and otherwise

$$FE_m = U_M + (\lambda^A - \lambda^S)\rho_L^2 - |J|\left(\frac{\rho_L}{\rho_M}\right)^{1/2} + FC \tag{26}$$

where F is the Faraday constant, C is the absolute potential of the reference electrode, and U_L and U_M are the absolute oxidation energies of P_L and P_M in situ, respectively, with $E_0 = U_M - U_L$; note that the corresponding midpoint-potentials $-U_L$, etc., were used in our previous study,[23] but the notation is changed slightly here to conform to more recent usages by others.[6] These equations have also been recently obtained by Müh.[61] Once the coefficients $|J|$ and $\lambda_A - \lambda_S$ are extracted by fitting experimental data to these equations, the individual values of the redox asymmetry for each mutant, as well as that for the wild-type, can be obtained using the observed values of ρ_L and ρ_M from

$$E_0 = |J|\left[\left(\frac{\rho_L}{\rho_M}\right)^{1/2} - \left(\frac{\rho_L}{\rho_M}\right)^{1/2}\right] - (\rho_L - \rho_M)(\lambda^A - \lambda^S) \tag{27}$$

Results obtained by applying eq 25 are shown in Figure 3 and are qualitatively similar but quantitatively distinct from the correlation obtained using the full four-state model. We see that, while these relationships are very helpful in providing a broad description of the chemical properties of the special pair, they are not suitable for quantitative analysis. Results obtained using both equations implicitly to generate the dependence of E_m on E_0 are shown in Figure 2A, exposing the basic weaknesses that lead to the errors depicted in Figure 3. Note that while Figure 2A shows that eqs 25 and 26 are continuous at their boundaries of validity, $E_0 = 0$, the two-root problem with adiabatic theory can also gives rise to an alarmingly sharp discontinuity in the expression for ρ_L at this point (i.e., in the correlation shown for low λ^A in Figure 2B) when λ^A becomes sufficiently large.

To understand the properties of systems such as these, it is important to extract the individual components λ_A and λ_S rather than just their difference. In principle, independent estimates of $|J|$ and the value of λ^S can be obtained by noting

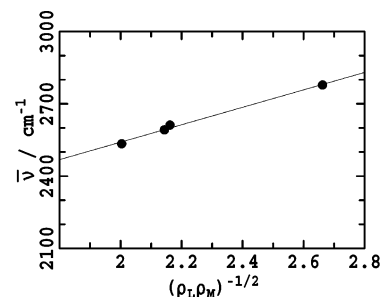(61) Müh, F., private communication.

Figure 7. Correlation between the observed average hole-transfer absorption energy ν_{av} (see Table 1) and the property $(\rho_L\rho_M)^{-1/2}$ of the internal charge distribution and its fit to a linear relation in accordance with eq 27.

that eq 22 implies that

$$h\nu_{\text{av}} = \lambda^S + \frac{|J|}{(\rho_L\rho_M)^{1/2}} \tag{28}$$

and hence correlating observed hole-transfer average band frequencies with observed spin densities. As for photosynthetic reaction centers, the vibronic-coupling scenario is near the worst-case condition for breakdown of the Born−Oppenheimer adiabatic assumption, and as we have demonstrated in Figure 2C that $h\nu_{\text{av}}$ is poorly represented by adiabatic theory, realistic values of $|J|$ and λ^S are not expected to be obtained from this procedure. Nevertheless, we plot $h\nu_{\text{av}}$ as a function of $(\rho_L\rho_M)^{-1/2}$ in Figure 7 for the wild-type and LH(M160), LH(L131), and LH(M160)+LH(L131) mutants. A linear correlation is obtained, but its slope gives $|J| = 0.045$ eV while its intercept is $\lambda^S = 0.23$ eV. These values are far from those obtained by full nonadiabatic simulation[31] of $|J| = 0.139$ eV and $\lambda^S = 0.003$ (for modes >200 cm^{-1}) or ca. 0.04 eV total.[26] Clearly, use of this procedure to estimate λ^S is also inherently unstable as the minimum value that the abscissa $(\rho_L\rho_M)^{-1/2}$ can take is 2, while the data must be extrapolated to zero abscissa to estimate λ^S.

7. Conclusions

Our four-state 70-vibration nonadiabatic model is shown to reproduce a wide range of properties of the special-pair radical cation of *Rb. sphaeroides* and 30 variants produced by site-directed mutagenesis. These include the observed average hole-transfer transition energy for all but one of the species considered and the electroabsorption Stark spectrum of the wild-type, all obtained through a priori prediction. In addition, the observed correlation between the observed midpoint-potential E_m and spin density ρ_L for 30 species belonging to six series of mutants is interpreted using three additional parameters that describe the absolute reference potential and geometrical factors relating the site of the mutation to the location of the two halves of the special pair. In all cases, application of our model was made on the basis of the assumption that the only influence of site-directed mutagenesis is to modify individually the redox potential of the (isolated) two halves of the special pair. While imperfections found between the predicted and observed properties could reflect inadequacies in our four-state model, in most cases it is clear that effects of mutation other than just the simple modulation of the isolated redox potentials are responsible for the major discrepancies. In particular, independent modulation of the energy of the SHOMO → HOMO state significantly affects the observed average transition energy.

As the parameters in our four-state model were either obtained from density-functional calculation[26] for the vibrational specifications or fitted to the observed phase-phonon plus hole-transfer spectrum for the six major control parameters including E_0, J, λ^A, and λ^S, further enhancements appear to demand refinement of the major parameters for each mutant. To achieve this, high-quality experimental difference spectra are required covering the whole of the observable spectrum of at least $300-5000$ cm^{-1}. The low-frequency part of the spectrum is particularly important as all physical properties derive from graphs of ϵ/ν as a function of ν rather than from the form of the extinction coefficient ϵ itself. Also, as the total intensity depends significantly upon the key control parameters, accurate measurement of the extinction coefficient is highly desired.

The values of parameters such as $J = 0.126 \pm 0.002$ eV, $\lambda^A = 0.139 \pm 0.003$ eV, and $E_0 = 0.069 \pm 0.002$ eV that appear in our four-state model are qualitatively similar but quantitatively distinct from other values recently obtained[6,7] through direct interpretation of the midpoint-potential E_m, spin localization ρ_L, and possibly also[7] band maximum (as an approximation to ν_{av}). Without use of hole-transfer band-energy information, unique solutions for the parameters are currently not attainable.[6] These interpretations are based[23] on Born$-$Oppenheimer adiabatic theory and ignore the presence of the SHOMO $\rightarrow$ HOMO state; they lead[7] to $|J| = 0.155$ eV and $\lambda^A = 0.22$ eV. Primarily, the differences between these values and those that appear in our general four-state model arise as the interpretation of ν_{av} requires a nonadiabatic approach[11,46] with also inclusion of the effects of the SHOMO $\rightarrow$ HOMO transition on the hole-transfer transition energy. That very simple analytical interpretations of the experimental data provide values of key quantities such as $|J|$ to within 25% of that obtained through elaborate calculations (taking 8 years to finalize[2,26,31] after their initial inception[45,46,59,62] involving an elaborate strategy[57]) indicates that the overall physical picture is soundly based.

While the interrelationships of the various directly observable chemical and spectroscopic properties appear convoluted, we have demonstrated the nature of the underlying more-simple dependencies on mutation-induced changes in the redox asymmetry E_0. This is particularly useful in isolating the scenarios in which the adiabatic approximation is expected to work well or fail badly. Further, we have presented a full range of adiabatic equations that, for the first time, include the effects of the symmetric modes on molecular properties. The importance of these equations lies primarily in providing a conceptual framework for the understanding of the means of control of photosynthetic processes exercised by site-directed mutagenesis of residues near the special pair. Quantitatively, however, bacterial photosynthesis is seen as a particularly poor application of two-state adiabatic theory as the SHOMO $\rightarrow$ HOMO state lies very close in energy to the hole-transfer state, and as the system is posed in the region of maximum nonadiabaticity with $2|J| \approx \lambda^A$. These effects may diminish for photosystem I reaction centers due to significant reduction of the coupling strength, making analytical approaches more reliable. A catastrophic failure of adiabatic theory will arise when $\rho_L \approx \rho_M$ in this system, however, due to the neglect of tunneling processes and the requirement that the ground-state adiabatic geometry change from one localized well to the other as shown in Figure 1B. The analytical equations provided are also generally applicable to ground-state organic and inorganic intervalence charge-transfer processes and are particularly apt if peripheral substituent effects can be employed to introduce controlled asymmetry in an otherwise symmetric environment, or if Stark spectroscopy can be employed for the same purpose.

(62) Reimers, J. R.; Hush, N. S. *J. Am. Chem. Soc.* **1995**, *117*, 1302.

JA036883M